

Cellular tension encodes local Src-dependent differential β_1 and β_3 integrin mobility

Richard De Mets^{a,†}, Irene Wang^{a,†}, Martial Balland^{a,†}, Christiane Oddou^b, Philippe Moreau^a, Bertrand Fourcade^a, Corinne Albiges-Rizo^b, Antoine Delon^{a,†,*}, and Olivier Destaing^{b,†,*}

^aLaboratoire interdisciplinaire de Physique, Université Grenoble Alpes et CNRS, 38402 Grenoble, Cedex, France;

^bInstitute for Advanced Biosciences, Centre de Recherche Université Grenoble Alpes, Inserm U 1209, CNRS UMR 5309, F-38700 La Tronche, France

ABSTRACT Integrins are transmembrane receptors that have a pivotal role in mechanotransduction processes by connecting the extracellular matrix to the cytoskeleton. Although it is well established that integrin activation/inhibition cycles are due to highly dynamic interactions, whether integrin mobility depends on local tension and cytoskeletal organization remains surprisingly unclear. Using an original approach combining micropatterning on glass substrates to induce standardized local mechanical constraints within a single cell with temporal image correlation spectroscopy, we measured the mechanosensitive response of integrin mobility at the whole cell level and in adhesion sites under different mechanical constraints. Contrary to β_1 integrins, high tension increases β_3 integrin residence time in adhesive regions. Chimeric integrins and structure–function studies revealed that the ability of β_3 integrins to specifically sense local tensional organization is mostly encoded by its cytoplasmic domain and is regulated by tuning the affinity of its NPXY domains through phosphorylation by Src family kinases.

Monitoring Editor

Valerie Marie Weaver
University of California,
San Francisco

Received: Apr 26, 2018

Revised: Oct 23, 2018

Accepted: Nov 16, 2018

INTRODUCTION

Extracellular matrix (ECM) mechanosensing is mainly supported by specialized heterodimeric transmembrane receptors called integrins. The function of these mechanoreceptors is based on their allosteric switch between open and closed conformations when activated by external or intracellular signals. Integrins form the adhesive core of nano- to microscale adhesion sites and perceive the chemical and mechanical cues from the ECM (Albiges-Rizo et al., 2009). Finally, integrin activation leads to the assembly and activation of intracellular signaling platforms implicated in mecha-

notransduction, cell survival, gene expression, and even the regulation of adhesion site dynamics.

Despite recognizing the same ECM protein, β_1 and β_3 integrins have different but cooperative activities in mechanoresponse (Schiller et al., 2013; Galior et al., 2016). Indeed, β_1 integrin plays a major role in force generation and transmission to the substratum (Roca-Cusachs et al., 2009; Lin et al., 2013; Rahmouni et al., 2013; Elloumi-Hannachi et al., 2015; Liao et al., 2015). In addition to negatively regulating cellular forces, β_3 integrins also regulate the clustering of β_1 integrins (Worth et al., 2010; Milloud et al., 2017). As integrin activity is based on cycles of activation and deactivation, their mobility oscillates between membrane free diffusion and transient immobilization events when linking the ECM and the matrix at adhesion sites (Cairo et al., 2006; Rossier et al., 2012; Leduc et al., 2013; Case and Waterman, 2015). These immobilization events are supported by multiple dynamic interactions with the numerous integrins partners that compose the adhesome (Schiller et al., 2013; Winograd-Katz et al., 2014; Horton et al., 2016). These multiple possible interactions explain why previous studies have unveiled that the integrin dynamic timescale spans orders of magnitude. Single-particle tracking (SPT) measurements highlighted fast diffusion (Rossier et al., 2012), whereas fluorescence recovery after photobleaching (FRAP) analyzed relatively slow integrin processes with a characteristic turnover time of tens to hundreds of

This article was published online ahead of print in MBoc in Press (<http://www.molbiolcell.org/cgi/doi/10.1091/mbc.E18-04-0253>) on November 21, 2018.

[†]These authors contributed equally to this work.

[‡]These authors contributed equally to this work.

*Address correspondence to: Antoine Delon (antoine.delon@univ-grenoble-alpes.fr); Olivier Destaing (olivier.destaing@univ-grenoble-alpes.fr).

Abbreviations used: CD, cytoplasmic domain; ECD, extracellular domain; ECM, extracellular matrix; FAK, focal adhesion kinase; FRAP, fluorescence recovery after photobleaching; MEF, mouse embryonic fibroblast; SFK, Src family kinases; SPT, single-particle tracking; tICS, temporal image correlation spectroscopy.

© 2019 De Mets et al. This article is distributed by The American Society for Cell Biology under license from the author(s). Two months after publication it is available to the public under an Attribution–NonCommercial–Share Alike 3.0 Unported Creative Commons License (<http://creativecommons.org/licenses/by-nc-sa/3.0>).

“ASCB®,” “The American Society for Cell Biology®,” and “Molecular Biology of the Cell®” are registered trademarks of The American Society for Cell Biology.

seconds (Ballestrem *et al.*, 2001; Cluzel *et al.*, 2005; Wehrle-Haller, 2007; Pines *et al.*, 2012).

To complete short-term SPT data, it is therefore interesting to analyze the ensemble-averaged mobility of integrins on a timescale of minutes and below the lifespan of adhesions (10 min). In addition, when evaluating the impact of each potential interaction, measuring mobility of integrins on a timescale of minutes is equivalent to integrate the resultants of their many cycles of free-diffusion/immobilization driven by their possible interactions in adhesion sites. These data could be particularly useful for determining the impact of mechanical tension on the strength of integrin interactions with partners. Indeed, the precise relationship between integrin mobility on a long timescale and the local tension applied on adhesive sites by the cytoskeleton is poorly understood. Using FRAP, Ballestrem *et al.* (2001) studied the density and turnover of $\beta 3$ integrins in single cells, demonstrating that these integrins exchange faster in high-density adhesions than in low-density adhesions, which are presumed to be less contractile. In *Drosophila* embryos, increased tension on muscle-tendon junctions decreases the mobile fraction of integrins measured by FRAP (Pines *et al.*, 2012).

Change of integrin dynamics raised the question of the potential existence of signaling pathways directly regulating this property. For instance, Src family kinases (SFKs) play an essential role in the signaling downstream of integrins by controlling the reinforcement of initial integrin-mediated adhesions, regulating focal adhesion turnover and activating numerous adaptors and kinases present in focal adhesions (Giannone and Sheetz, 2006; Huvneers and Danen, 2009; Destaing *et al.*, 2011).

To investigate the link between integrin mobility on a long timescale and the local tension applied on adhesive sites, we propose to create stable and reproducible regions of adhesion sites under different levels of tension while simultaneously measuring integrin dynamics. Modulation of the cellular mechanoresponse is often induced by changing hydrogel rigidity where the ECM is adsorbed. However, this modulation might also alter hydrogel porosity, which can affect the presentation of the ECM (Arnold *et al.*, 2008; Trappmann *et al.*, 2012). Conversely, adhesive micropatterns on glass allow the control of cell shape, thus providing well-controlled mechanical zones with different stress fiber organization and tension (They *et al.*, 2006; Tseng *et al.*, 2011; Mandal *et al.*, 2014). In addition, micropatterning allows the observation of focal adhesions at steady state and reduces the possible bias of their maturation on integrin molecular mobility. Therefore, to observe local changes of integrin mobility in adhesion sites under different tensional environments, we combined micropatterning and simultaneous molecular mobility measurements in different regions of the same cells. The choice of the approach to measure molecular mobility depends on the temporal resolution achieved. Although SPT provides high-precision molecular dynamics, it is a challenge to correlate this information to multiple cellular structures at the whole cell level (Rossier *et al.*, 2012; Jaqman *et al.*, 2016). In addition, due to photobleaching and blinking of photoconvertible probes (Bourgeois *et al.*, 2012; Ha and Tinnefeld, 2012), SPT is better suited for fast dynamics (subsecond). To measure integrin mobility over long time periods and at the whole cell level, temporal image correlation spectroscopy (tICS) is used to extract the long-residence time and the density of fluorescent probes from time-lapse series of images (Bachir *et al.*, 2014; Hoffmann *et al.*, 2014; Kolin *et al.*, 2006; Kolin and Wiseman, 2007). This approach extends the principle of fluorescence correlation spectroscopy on images (two dimensional) and has been used to study the mobility of integrins and adhesion

molecules, such as paxillin, during focal adhesion maturation (Chen *et al.*, 2012; Toplak *et al.*, 2012).

Here we investigate how intracellular tension directly affects the mobility of $\beta 1$ and $\beta 3$ integrins. Our tICS data on integrin dynamics reveal the existence of at least two long dissociation times. Weakly bound and “immobilized” populations of integrins can be found in adhesion sites and outside adhesions. In marked contrast to $\beta 1$ integrins, we demonstrate that the residence time of the $\beta 3$ integrins as measured by tICS depends on the local tensional level with high tension increasing the residence time. Based on the difficulties encountered when modulating contractility at the subcellular level by pharmacological approaches, reverse genetic and micropatterning are used to reveal that the mechanosensitivity of mobility is encoded and regulated by the dynamic phosphorylation of the distal and proximal Asn-Pro-X-Tyr (NPXY) motifs in the cytoplasmic domain of $\beta 3$ integrins. Only a kinase binding directly to the SFKs can directly regulate the dynamic phosphorylation of the distal and proximal NPXY domain of $\beta 3$ integrins.

RESULTS AND DISCUSSION

Arrow micropatterns induce modulation of intracellular tension in different regions within single cells

Among different micropatterns of fibronectin, the arrow shape is selected given that it induces the best contrast of cytoskeletal tension in separate regions of single mouse embryonic fibroblast (MEF) cells (Figure 1 and Supplemental Figure 1). Since all analyzed cells have a normalized organization (Supplemental Figure 2), the average fluorescence intensity for each actoadhesive element is used to quantify the spatial distribution of molecular recruitment over a cell population.

First, phosphotyrosine staining, a classical marker of focal adhesion, reveals that adhesion sites are localized at each corner without significant differences in staining intensity between the head and tail of the arrow (red A–B dashed line, Figure 1a). F-Actin images reveals two types of stress fibers. Nonsupported stress fibers (NSFs) between the barb and the tail of the arrow (C position in the red dashed line, Figure 1a) are more intense than supported stress fibers between the barb and the head of the arrow (D position in the red dashed line, Figure 1a). As expected, NSFs also accumulate 50% more phosphomyosin light chain (Phospho-MLC) compared with supported stress fibers, indicating that they are more contractile. NSF formation between nonadhesive corners is consistent with previous studies demonstrating that these fibers are associated with higher tension (Tseng *et al.*, 2011; Mandal *et al.*, 2014). To confirm that this micropattern strategy also significantly modulates tension applied on adhesive sites, the recruitment of mechanosensitive adhesive molecules, including vinculin and phosphorylated paxillin, is monitored (Plotnikov *et al.*, 2012; Case *et al.*, 2015). Both the recruitment of vinculin and the phosphorylation of paxillin are increased by 30% in the tail of the arrow, where large contractile nonsupported stress fibers are anchored (F position in the red dashed line, Figure 1a).

On a 5-kPa soft substrate, we observed the same asymmetric distribution of NSF, phospho-MLC, vinculin, and phosphopaxillin as on glass (Supplemental Figure 3a). Traction force microscopy is performed with these patterns to quantify the mechanical stress applied to the substratum. We observe a 20% increase in traction stress on the substratum at the tail compared with the head of the arrow (blue region, Supplemental Figure 3b). This finding demonstrates that traction force distribution is consistent with the anisotropic pattern-induced modulation of cytoskeletal tension.

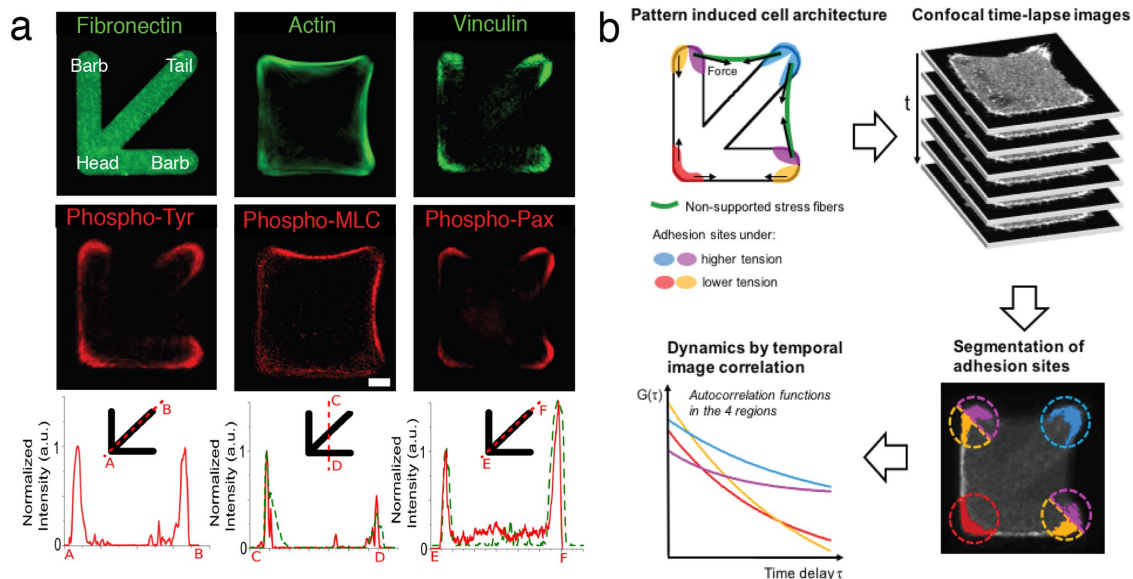


FIGURE 1: Arrow micropatterns control intracellular tension localization and asymmetric distribution of mechanosensitive adhesions proteins. (a) Average images over 37 MEF cells spread on fibronectin arrow micropatterns on glass of a general marker of adhesion sites (Phospho-Tyr), mechanosensitive proteins, and actomyosin cytoskeleton. Normalized fluorescence intensity analysis over the indicated dashed red line showed that classical mechanosensitive proteins such as vinculin and phospho-paxillin are enriched in the tail of the arrow confirming an increase of local intracellular tension in this region. (b) Scheme of the principle of our experimental approach. Spreading of cells on micropatterned arrows allowed to induce regions with different intracellular tensions that can be segmented to measure integrin mobility by tICS analysis there. Besides analysis the mobility at the whole cell level, tICS analysis on micropatterns allows us to average mobility data on numerous cells in the same conditions. Scale bar = 3 μm .

In summary, our arrow-shaped micropattern strategy allows the generation of different and reproducible levels of intracellular tension and transmitted forces within the same cell in a spatially controlled manner. Thus, this strategy allows us to study the corresponding integrin dynamics.

Cells stably expressing green fluorescent protein (GFP)-tagged integrins and spread on arrow micropatterns are imaged by time-lapse confocal images at their basal surface with 1-s temporal resolution. On each cell, regions in which adhesions are submitted to different levels of tension are segmented and analyzed by tICS, which provides information on the density and residence time of integrins (Figure 1b). Given that measurements are performed simultaneously in different regions of the same cell, we can monitor and compare integrin dynamics with high sensitivity in response to different levels of local mechanical stress.

Model and tICS analysis

We aim to study the mechanosensitive dynamical properties of $\beta 1$ and $\beta 3$ integrins independently of focal adhesions reorganization. Thus, probing these dynamics below the lifespan of adhesions is a well-suited timescale. Henceforth, our analysis is based on a simplified model that integrates a complex network of interactions (Pines *et al.*, 2012). The model assumes that integrins in focal adhesions (see Figure 2) can be observed in three different dynamical states: 1) first state, free diffusion within the membrane (with a coefficient of $\sim 0,1 \mu\text{m}^2/\text{s}$); 2) second state, binding and unbinding (characterized by a residence time $t_{\text{off}} < 200 \text{ s}$); and 3) third state, immobile integrins (i.e., bound for times $>$ the acquisition time = 200 s). We thus designed an experiment capable of detecting dynamic molecular events of characteristic times from 1 to $\sim 200 \text{ s}$, at the whole-cell level. The tICS modality fulfills the corresponding requirements,

because it provides image stacks over several minutes at a frame rate of approximately one image per second. At this speed, the lateral diffusion time of integrins, which is $< 0.1 \text{ s}$ (Rossier *et al.*, 2012), is too fast to be observed given that it is shorter than the temporal resolution (Figure 2). Conversely, the so-called immobile integrins leave a footprint in temporal image correlation because the latter is based on ensemble averages over a given region of interest (Kolin *et al.*, 2006). The immobile fraction thus appears as a constant offset of the correlation function that does not decay to the no-correlation level at long times (200 s) as displayed in Figure 2. The tICS correlation functions were fitted with an exponential decay to yield the residence time t_{off} that describes the intermediate time behavior (1 to $\sim 200 \text{ s}$) (Fourcade, 2017). We stress the fact that this time is not characteristic of a single interaction between an integrin molecule and a given partner but is rather an effective time that integrates an entire set of interactions that link integrins to other adhesion components and the actin cytoskeleton. Our model ignores integrins trafficked from the plasma membrane to the cytosol by endocytosis because the latter process mostly occurs on timescales of tens of minutes and under low tension (Yu *et al.*, 2015).

To conclude, tICS analysis offers the advantages of measuring integrin mobility in regions of arbitrary shape, independently of geometrical parameters.

Intracellular tension affects $\beta 3$ -GFP integrin mobility but not $\beta 1$ -GFP integrins mobility in adhesion sites

To monitor all integrins of a chosen type, $\beta 3$ -GFP or $\beta 1$ -GFP is re-expressed in MEF knockout cells for the considered integrins (i.e., $\beta 3^{-/-}$ MEF or $\beta 1^{-/-}$ MEF cells, respectively). Only adhesion sites displaying a typical lifespan greater than 10 min as observed by live imaging are studied (unpublished data). Within each cell, five

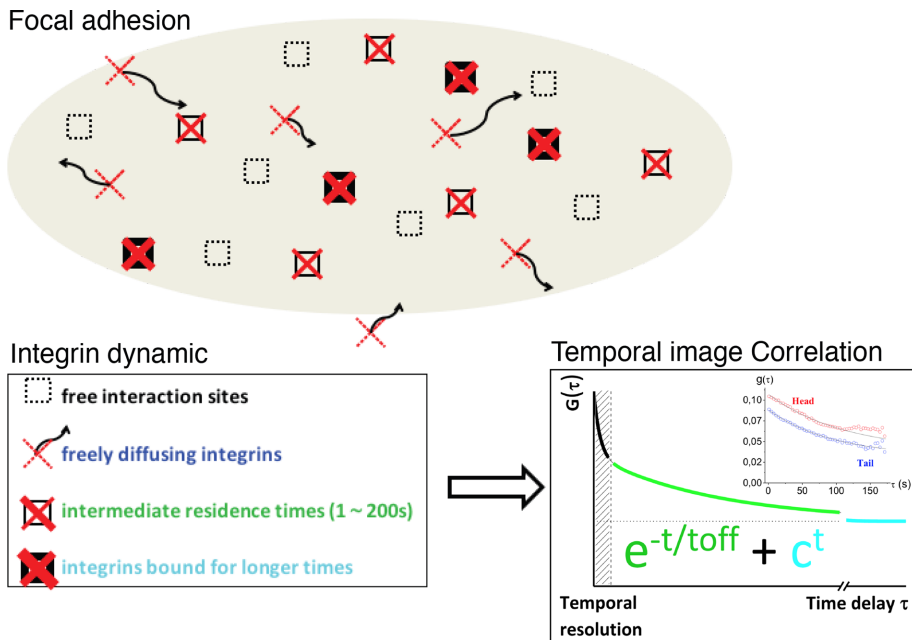


FIGURE 2: Mobility model to analyze tICS data. Scheme of a focal adhesion that contains three subpopulations of integrins: freely diffusing integrins; integrins bound on interaction sites for times shorter than the observation time (200 s) and integrins bound at longer time. Since diffusion is too fast to be observable, given the temporal resolution of the tICS data (1 s), the latter have a characteristic decay time that corresponds to the unbinding rate. The immobile integrins contribute to the correlation curves through the offset that persists at longer times. Typical sample of temporal image correlation plots for $\beta 3$ -GFP in the head (red) and tail (blue) of arrow pattern were associated with the theoretical scheme of temporal image correlation scheme.

regions are analyzed after segmentation, including a region outside adhesions (black) and four adhesion regions, including at the arrow tail (blue), on the side of the barbs oriented toward the tail (violet), on the side of the barbs oriented toward the head (orange) and

at the arrowhead (red). TICS correlation functions (Figures 1 and 3) are computed for these five regions and fitted separately using the interaction model presented above. Strikingly, tICS measurements indicate complex dynamics in all regions. Indeed, all correlation functions exhibit an initial exponential decay corresponding to integrin unbinding with intermediate rates (dissociation times of tens to hundreds of seconds) plus an offset value indicating the presence of integrins engaged in long-lived interactions (dissociation times greater than 200 s). In other words, these data demonstrate the existence of two subpopulations of integrins: one in dynamic interactions and another that remains bound during the observation period.

We then compared the dissociation time of dynamic integrins in the different regions. First, the residence times measured inside adhesion sites are longer (>90 s) than those measured outside adhesions (40 s) for both integrins. This finding is expected given that the integrins undergo more stable interactions in adhesive sites. More interestingly, the dependence of integrin dynamics on the mechanical environment differs between the two types of integrins. $\beta 3$ -GFP residence time (τ_{off}) increases significantly from adhesion sites under low intracellular

tension (red and orange) and those under higher intracellular tension (violet vs. blue) on the head side and tail side of the arrow, respectively (τ_{off} varies significantly from 90 to 150 s, Figure 3b). Importantly, the effect of intracellular tension on $\beta 3$ -GFP dynamics is

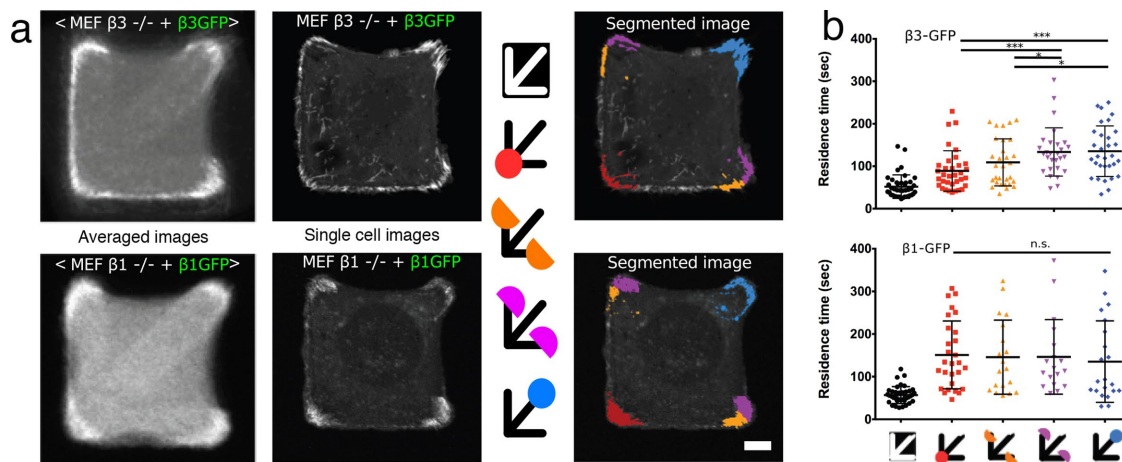


FIGURE 3: Intracellular tensions encodes differently $\beta 1$ and $\beta 3$ -GFP integrins mobility in adhesion sites. (a) Averaged confocal images over 32 cells spread on glass of MEF $\beta 3^{-/-}$ reexpressing $\beta 3$ -GFP or MEF $\beta 1^{-/-}$ reexpressing $\beta 1$ -GFP spread on glass arrow micropatterns. Adhesion sites in regions of the arrow patterns with different levels of tension are segmented and analyzed separately by tICS. All the fluorescence acquired inside the arrow micropattern but outside FAs is used to analyze integrin mobility outside adhesions (black). (b) Quantification of the residence time of $\beta 3$ -GFP and $\beta 1$ -GFP in each adhesion site segmented and color coded as previously. These measurements were extracted from tICS analysis of 3 min image series over ~30 cells. Both $\beta 3$ -GFP and $\beta 1$ -GFP residence times increase between nonadhesion (in black) and adhesion (all colors) sites. $\beta 3$ -GFP residence time significantly increases between head (red) and tail (blue) of the arrow micropatterns, showing that higher intracellular tension increases $\beta 3$ -GFP residence time. $\beta 1$ -GFP residence time is not sensitive to change in intracellular tension as it remains unchanged in the different adhesion sites. Scale bar = 1 μ m.

extremely local given that significant differences are found in neighboring regions of the same barb (orange and violet) attached to fibers with different contractile activity. In contrast, $\beta 1$ -GFP integrins do not appear to respond to modulation of intracellular tension in the same range as $\beta 3$ -GFP (Figure 3b), demonstrating the specific mechanosensitive behavior of $\beta 3$ -GFP integrins. Indeed, the residence time of $\beta 1$ integrins remains ~ 150 s independently of the level of tension in adhesion sites.

The observed dependence of the residence time on intracellular tension requires a discussion of the molecular basis supported by these types of measurements. Indeed, we measured a residence between 40 and 160 s that is much larger than the characteristic integrin times measured by SPT (Rossier *et al.*, 2012). In parallel to SPT measurements focused on short-time-scale and isolated integrin behaviors, the tICS approach allows measurements of an average residence time that is due to the collective resultant of the mobility behavior of hundreds of integrins experiencing numerous interactions. Thus, tICS is complementary to SPT analysis because it allows the connection of mobility analysis in another time window during the adhesion lifespan and at the whole cell level. An increase in the residence time indicated that $\beta 3$ integrins are more strongly bound in adhesion sites submitted to higher tension, whereas $\beta 1$ integrin behavior does not depend on mechanical tension. Our results are not consistent with previous FRAP experiments demonstrating a faster turnover of $\beta 3$ -GFP in focal adhesions containing a high density of integrins where contractility is thought to be high (Ballestrem *et al.*, 2001). However, this discrepancy might result from the high variability of FRAP experiments, especially when the measured adhesions could be still maturing compared with the adhesions considered on arrow-shaped micropatterns that are in their steady state.

The different mechanosensitivity between $\beta 1$ and $\beta 3$ integrins raises the question of the functional relevance of the tuning of their residence time. This fine-tuning is supported by a theoretical model proposing that rigidity sensing could be supported by at least two integrins with different binding/unbinding rates to the ECM (Elosegui-Artola *et al.*, 2014). Changing the mobility of integrins will directly affect the associated signaling and the mechanical properties of their connected cytoskeleton. For instance, $\beta 3$ integrins activate the actin bundler formin mDia1, whereas $\beta 1$ integrins activate the contractile RhoA-Rock-MyoII pathway (Schiller *et al.*, 2013).

Dynamic interactions of $\beta 3$ integrin NPXY domains are required for the mechanosensitive response

Our next challenge is to determine the molecular basis of the link between the regulation of integrin mobility and intracellular tension. In our conditions, the use of classical pharmacological approaches (Y27632 or blebbistatin) inhibits the formation of focal adhesions of cells spread on the arrow patterns (unpublished data). This feature makes it difficult to compare integrin mobility in normal and highly perturbed focal adhesions. Thus, to correlate integrin mobility with local tension and contractility tuning, we used reverse genetic to elucidate which integrin domains dictate its residence time and are responsible for the different mechanosensitive behaviors of $\beta 1$ and $\beta 3$ integrins. To determine the role of the extracellular (ECD) and cytoplasmic (CD) domains of $\beta 3$ -GFP for mechanosensitivity, tICS experiments are performed on integrin chimeras by switching the cytoplasmic domain between $\beta 1$ and $\beta 3$ integrins (Figure 4a). The residence time of $\beta 1$ ECD- $\beta 3$ CD responds to forces in a manner similar to that of $\beta 3$ -WT, whereas $\beta 3$ ECD- $\beta 1$ CD is similar to that of $\beta 1$ -WT. Thus, it appears that the residence time relies exclusively on the short cytoplasmic domain of the integrin in response to changes

in intracellular tension and not on the interaction of the ECD with the ECM (Figure 4b). This notion is reinforced by the fact that a $\beta 3$ -GFP integrin mutant that binds more efficiently the ECM (N304T/S) behaves like $\beta 3$ -WT (Supplemental Figure 4). Indeed, although its extracellular conformation is different, this mutant maintains the same ability to bind cytosolic partners. Based on these mutants, it appears that the integrin residence time we observe is under the control of cytosolic interactions.

Then, to describe the molecular basis of this mechanomodulation, we focus on the proximal and distal NPXY domains of $\beta 3$ integrins that are involved in their binding with the activators, talins and kindlins. To compare the behaviors of different integrin mutants with different affinities for these proteins, we first investigate whether talin or kindlin recruitment is mechanosensitive. Contrary to vinculin or phospho-paxillin (Figure 1), talins or kindlins do not present any specific enrichment in high intracellular tension regions (Supplemental Figure 5). Mutation of the tyrosine into alanine of the proximal (Y772A) or distal (Y784A) NPXY domains abolishes the interaction with talins and kindlins, respectively (Figure 4c) (Schaffner-Reckinger *et al.*, 1998, 2001; Brakebusch *et al.*, 2000; Calderwood *et al.*, 2003; Czuchra *et al.*, 2006; Anthis *et al.*, 2009; Bledzka *et al.*, 2010). Consistently, these mutants fail to be recruited at adhesion sites (Figure 4d) and exhibit the same short residence time in the presumed adhesion areas (head-red and tail-blue) defined in $\beta 3$ -GFP WT as outside the adhesion sites (< 50 s, Figure 4d). However, their expression does not affect the difference in tension between the head and tail induced by the arrow pattern as large NSF are still formed. Therefore, it is likely that the partners of both NPXY domains cooperate to immobilize integrins in adhesion sites. This led us to consider other mutants that do not block the recruitment of NPXY-binding partners of $\beta 3$ integrins but rather increase the lifetime of their interactions. Y772F or Y784F mutants of $\beta 3$ integrin can still bind talins and kindlins, respectively, but these interactions are no longer inhibited on the phosphorylation of the missing tyrosine. In addition, the lifetime of these interactions with $\beta 3$ integrin are probably increased (Oxley *et al.*, 2008; Bledzka *et al.*, 2010; Deshmukh *et al.*, 2010). Interestingly, we demonstrate that Y772F or Y784F mutants exhibit increased residence time in the head of the arrow (~ 150 s) but not in the tail (Figure 4d), demonstrating the key importance of the tyrosine phosphorylation of these NPXY domains for the mechanosensitive mobility of $\beta 3$ integrin. Thus, it appears that mechanomodulation of $\beta 3$ integrin could be controlled by the activity of the kinase(s) targeting these NPXY domains (Giannone and Sheetz, 2006).

SFK activity controls the mechanosensitive mobility of $\beta 3$ -GFP integrins

Focal adhesion kinase (FAK) and SFKs have a prominent role in adhesion site mechanotransduction (Giannone and Sheetz, 2006; Huvneers and Danen, 2009; Destaing *et al.*, 2011). However, to date, no direct role of these kinases on integrin mobility has been reported. We explore their roles by pharmacologically inhibiting Src or FAK kinase activities with 10 μ M Src inhibitor PP2 or FAK inhibitor (FAKi) 30 min prior to tICS imaging (Figure 5a and Supplemental Figure 6). Neither FAKi nor PP2 (Src inhibitor) affects $\beta 3$ -GFP accumulation in adhesion sites or cell spreading on the arrow-shape micropattern (Figure 5a).

Src inhibition but not FAK abolishes the differential residence time of $\beta 3$ -GFP between low and high-tension regions (Figure 5b). This treatment results in a behavior similar to that of $\beta 3$ -Y784F and $\beta 3$ -Y772F mutants that also present equal mobility values between the head and tail (Figure 4d). Thus, inhibiting Src kinase

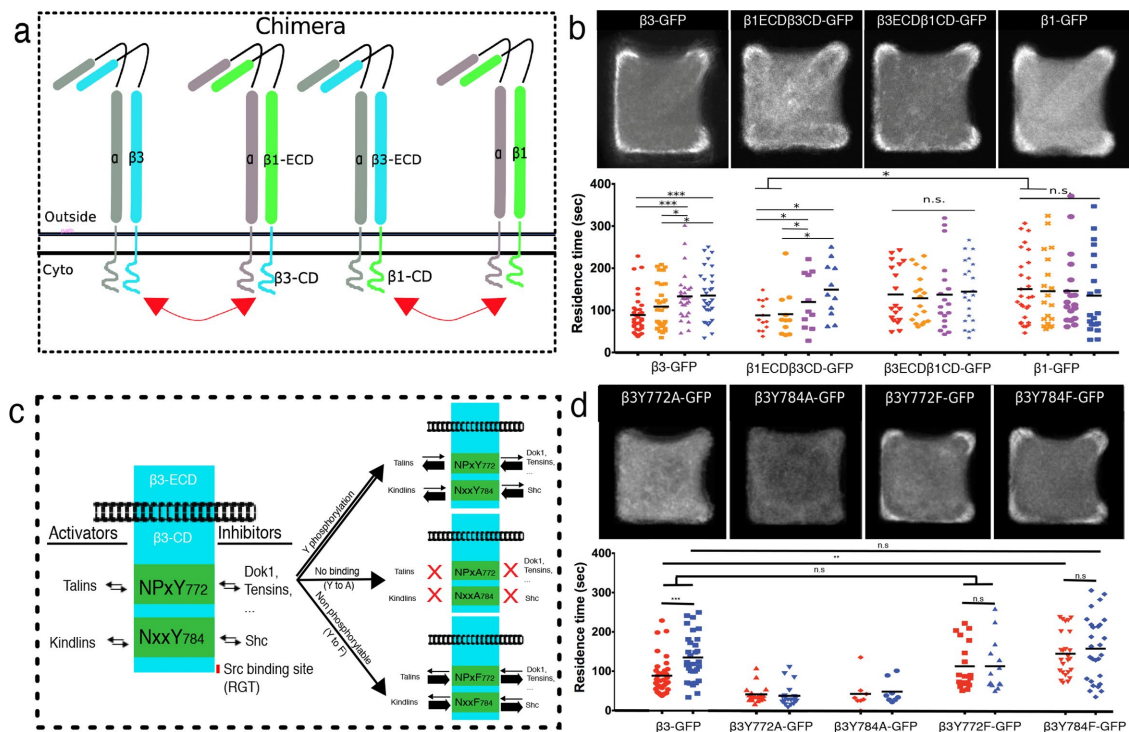


FIGURE 4: Mechanosensitive mobility of $\beta 3$ -GFP integrins is encoded by its short cytoplasmic domain and under the control of dynamic interactions regulated through the phosphorylation of the NPXY domains. (a) Scheme of β chain integrin chimeras used and reexpressed in MEF $\beta 3^{-/-}$ cells. ECD of $\beta 1$ was associated with the transmembrane and CD of $\beta 3$ while the ECD of $\beta 3$ was associated with the transmembrane and CD of $\beta 1$. (b) Averaged images and segmentations over 28 cells spread on glass of MEF $\beta 3^{-/-}$ reexpressing $\beta 1$ -GFP, $\beta 3$ -GFP, $\beta 1$ ECD- $\beta 3$ CD-GFP, or $\beta 3$ ECD- $\beta 1$ CD-GFP spread on glass arrow micropatterns. Quantification of the residence time of these chimeras in each adhesion site segmented and color-coded as previously shows that the ECD of $\beta 1$ was not sufficient to inhibit mechanosensitive mobility of the CD of $\beta 3$. Moreover, replacement of the CD of $\beta 3$ by the CD of $\beta 1$ is sufficient to abolish the mechanosensitive response of $\beta 3$ -GFP and to induce the characteristic behavior of $\beta 1$ -GFP residence time. (c) Averaged images and quantification over ~30 cells spread on glass of MEF $\beta 3^{-/-}$ reexpressing GFP-tagged mutants that cannot bind talin (Y772A), that cannot bind kindlin (Y784A), that can bind talin but cannot regulate this interaction through phosphorylation (Y772F) and that can bind kindlin but cannot regulate this interaction through phosphorylation (Y784A). Both $\beta 3$ Y772A-GFP and $\beta 3$ Y784A-GFP were poorly retained in the adhesion sites and present the same dynamics as $\beta 3$ -GFP outside adhesion sites. Both $\beta 3$ Y772F-GFP and $\beta 3$ Y784F-GFP mutants lose the ability to modulate their residence time with the level of tension. However, while $\beta 3$ Y772F-GFP stays rather mobile, $\beta 3$ Y784F-GFP mutant behaves in all regions as in high tension adhesion sites, by presenting enhanced immobilization. Scale bar = 3 μ m.

activity mimics mutants with a nonphosphorylatable NPXY motif, which is consistent with previous observations of SFK-dependent $\beta 3$ integrin phosphorylation (Law *et al.*, 1996, 1999; Datta *et al.*, 2002). To move beyond pharmacological approaches, $\beta 3$ integrin mutants that are affected in FAK or Src binding were examined (Figure 5c). Both D748A and E751A mutations inhibit the interaction with FAK (Schaller *et al.*, 1995), whereas the deletion of the final RGT sequence abolished the binding of $\beta 3$ integrin with the SH3 domain of Src (Arias-Salgado *et al.*, 2003). Consistent with FAKi treatment, perturbing the $\beta 3$ -FAK interaction does not affect the mechanosensitive response of $\beta 3$ -GFP (Figure 5d). In contrast, inhibition of Src binding to $\beta 3$ -GFP abolishes $\beta 3$ -GFP mechanosensitivity. This mutation does not block the accumulation of $\beta 3$ -GFP inside the focal adhesion but rather inhibits the modulation of its residence time. Therefore, abolishing either the interaction of $\beta 3$ with Src or the kinase activity of Src similarly desensitizes $\beta 3$ -GFP mobility to intracellular tension. However, the $\beta 3$ -GFP Δ RGT mutant exhibits reduced global residence time in high-tension regions compared with the $\beta 3$ -Y784F-GFP mutant or PP2 treatment (Figure 5d). This discrepancy could be explained by dif-

ferent functions of the adaptor and the kinase activities of SFKs on $\beta 3$ -GFP mobility (Schwartzberg *et al.*, 1997). Indeed, the binding of the SH3 domains of SFKs to integrins could be essential to increase the residence time of $\beta 3$ -GFP only in high-tension regions by competing with kindlins for the binding to $\beta 3$ -GFP, reducing its activation. Indeed, recent data demonstrated that the RGT domain could also bind with kindlins (Liao *et al.*, 2015). Although our data demonstrate that the RGT domain is not as important as the membrane distal NPXY domain for kindlin binding, its deletion may only slightly impair its binding with kindlins and affect its residence times in adhesion sites compared with the $\beta 3$ -Y784F-GFP mutant or PP2 treatment.

Our identification of Src as a key player in the mechanosensitivity of integrin mobility could partially explain the reason why $\beta 3$ and not $\beta 1$ integrin residence time is sensitive to tension. Indeed, $\beta 1$ integrins do not harbor the RGT domain and therefore do not interact with Src (Arias-Salgado *et al.*, 2003).

Combining micropatterning to control mechanical constraints in different regions with integrin dynamics measurements by tICS made it possible to demonstrate that intracellular tension

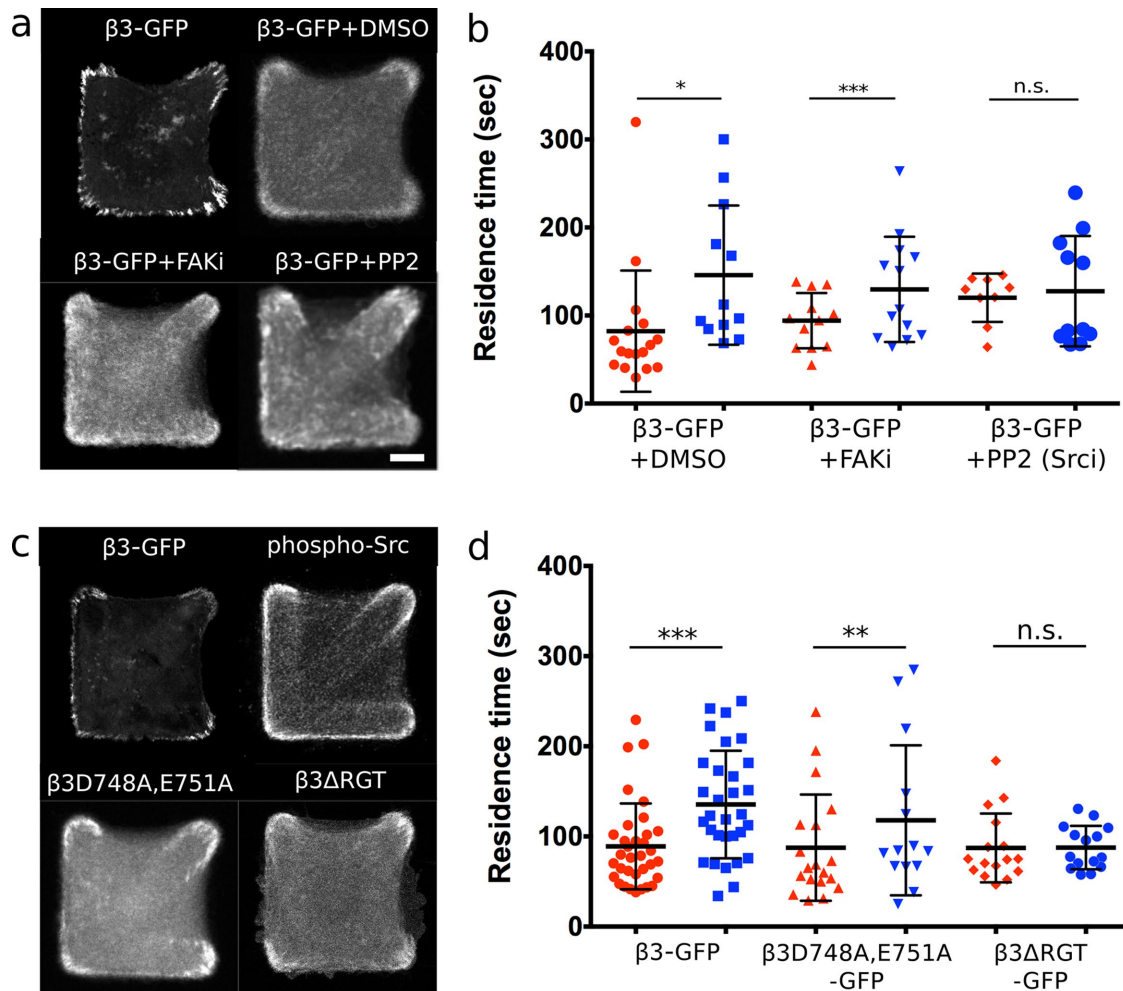


FIGURE 5: SFK inhibition mimics the absence of mechanosensitive mobility as found in mutants with nonphosphorylatable NPXY domains. (a) Averaged images of $\beta 3$ -GFP over 23 cells (MEF $\beta 3^{-/-}$ reexpressing $\beta 3$ -GFP) spread on glass in four conditions: untreated, treated with DMSO, FAKi and SFK inhibitor (PP2) at 10 μ M for 1 h before imaging. (b) Quantification over ~23 cells of the residence time of $\beta 3$ -GFP during inhibition of two important kinases in adhesion site dynamics, FAK and SFK. FAK inhibition does not affect the mobility of $\beta 3$ -GFP while SFK inhibition increases $\beta 3$ -GFP residence time in low tension regions (head of the arrow micropatterns) and abolishes the modulation of $\beta 3$ -GFP residence time in response to increase of intracellular tension. (c) Averaged images and (d) quantification of the residence time over 23 cells spread on glass of MEF $\beta 3^{-/-}$ reexpressing $\beta 3$ D748A, E751A-GFP that cannot bind two main regulators of adhesions sites, FAK and paxillin, and MEF $\beta 3^{-/-}$ reexpressing $\beta 3$ - Δ RGT-GFP that cannot bind SFKs. In the absence of binding with FAK and paxillin, $\beta 3$ D748A, E751A-GFP is still able to modulate its residence time in response to increase of intracellular tension. On the contrary, inhibiting Src- $\beta 3$ integrin binding completely abolished the modulation of $\beta 3$ integrins residence time in response to an increase of intracellular tensions. (d) Differential sensitivity of $\beta 1$ and $\beta 3$ integrin mobilities in response to global and local changes of intracellular tension is regulated by Src activity. Scale bar = 3 μ m.

differently affects the activation cycles of $\beta 1$ and $\beta 3$ integrins. Our structure–function study revealed that the ability of $\beta 3$ integrin to sense local tension is based on the dynamic tuning of its NPXY domains. The different importance of the NPXY domains of $\beta 1$ and $\beta 3$ integrins in mechanoreponse is an additional experimental observation supporting the theoretical model proposing that different binding and unbinding rates of two integrin types can regulate traction forces by affecting the transmission of forces generated by the intracellular actin flow (Elosegui-Artola *et al.*, 2014).

Thus, our data highlight a new pathway for mechanotransduction where SFK controls $\beta 3$ integrin residence time in response to changes in mechanical stress.

MATERIALS AND METHODS

Cell culture and infection

MEF were grown in DMEM (4.5 g/l glucose, with glutamine; PAA Laboratories GmbH) supplemented with 10% (wt/vol) fetal bovine serum and penicillin/streptomycin. $\beta 3^{+/+}$ integrin and $\beta 3^{-/-}$ integrin MEFs were the generous gift of Richard Hynes (The David H. Koch Institute for Integrative Cancer Research, Massachusetts Institute of Technology, Cambridge, MA). MEF isolated from $\beta 1^{loxP/loxP}$ mice between embryonic day 12 and postnatal day 1, as described recently (Ferguson *et al.*, 2009), were the generous gift of Reinhard Fässler (Max Planck Institute of Biochemistry, Martinsried, Germany). At least five clones from five floxed mice were isolated and mixed. Cre

recombinase expression was achieved by adenovirus transduction and the respective adenoviruses were purchased from the University of Iowa Gene Transfer Vector Core (Iowa City, IA). Maximal $\beta 1$ depletion was achieved within 4–6 d. Cells were then fluorescent-activated cell sorting (FACS)-sorted based on their $\beta 1$ expression to obtain a large and pure population of MEF $\beta 1^{-/-}$. Rescue of integrin was achieved by retroviral infection using pFB-Neo-human $\beta 1$ -GFP or pBabe-mouse $\beta 3$ -GFP vectors, which were generous gifts from M. Humphries (University of Manchester, England) and B. Wehrle-Haller (University of Geneva, Switzerland). cDNAs delivered by retroviral transduction following packaging in Phoenix-Eco cells (American Type Culture Collection, Manassas, VA). The supernatant containing viral particles from transduced cells was harvested, filtered, and following addition of 8 $\mu\text{g}/\text{ml}$ polybrene (Sigma-Aldrich), was used to infect either $\beta 1^{-/-}$ or $\beta 3^{-/-}$ fibroblasts, as previously described (Destaing *et al.*, 2010). Rescued cells were then FACS-sorted to obtain knockout cells with surface integrin levels comparable to those of the parental cells.

Mutagenesis

pBabe-mouse $\beta 3$ -GFP, pBabe-mouse $\beta 3\text{D}748\text{A}$, E751A-GFP, pBabe-mouse $\beta 3\text{Y}772\text{F}$ -GFP, pBabe-mouse $\beta 3\text{Y}784\text{F}$ -GFP and pBabe-mouse $\beta 3\text{R}785\text{stop}$ -GFP constructs were generated using a Quickchange XL site-directed mutagenesis kit (Stratagene, La Jolla, CA) using the following sense primers:

W740A: 5'-ctgctactctgctcatcGCGaagctactcatcactatc-3'; D748A+E751A: 5'catcactatccatGCCcggagGCAAttgctaaattgagg-3'; Y772F: 5'cagcaacaaccgctgTTTaaagaggccactccacc-3'; Y784F: 5'cctccacctcacaatataccTTCcgggggac-3'.

Deletion of the RGT motif (R785) was achieved using the Gibson assembly cloning kit (New England Biolabs, Ipswich, MA) with the following primers:

5'cat aga aga cac cga ctc tag agG ATC CCC CGG GCT GCA GG-3' with 5'GGT GGC GAC CGG TGA ttt tcc ctc GTA GGT GAT ATT GGT G-3' and

5'CAC CAA TAT CAC CTA Cga ggg aaa aTC ACC GGT CGC CAC C-3' with

5'cca gag gtt gat tgt cga cga att cTT ACT TGT ACA GCT CGT CCA TG-3'.

Reagents and antibodies

Antibodies for immunofluorescence were obtained from the following commercial sources: rat anti-activated $\beta 1$ integrin (9EG7; BD Pharmingen), rabbit anti-mouse Talin (homemade clone J61; described in Martel *et al.*, 2001) and mouse anti-rat Kindlin2 (clone 3A3; Millipore, Fremont, CA), rabbit anti-phospho-paxillin PY118 (Invitrogen), mouse anti-Vinculin (11-5; Sigma), phalloidin-TRITC (LifeTechnology), mouse anti-phospho-tyrosine (4G10; Millipore), rabbit anti-phospho-MLC (Cell Signaling), anti-416phosphoSrc (Cell Signaling). Alexa 647 and 546 conjugated secondary antibodies were purchased from Invitrogen.

Src and FAK inhibition experiments were performed at 10 μM final of PP2 (Sigma) and FAKi (Selleckchem) on MEF $\beta 3^{-/-}$ $\beta 3$ -GFP spread on patterns.

Micropatterning and cell spreading

Control of the cell geometry was made by grafting patterns of nonadhesive PNIPAM brushes on coverslips of 32 mm diameter (Bureau and Balland, 2014). The adhesive surface of cells was determined manually with ImageJ software, using the contour of

phase contrast image. Adhesive patterns had an arrow shape with bars 32 μm long and 6 μm wide embedded in a total square surface of 1024 μm^2 .

Cells (50,000) were plated on coverslips coated with fibronectin (20 $\mu\text{g}/\text{ml}$) 4 h before imaging. Observation media was a modified version of DMEM without NaCO_3 , pyruvate, and red phenol and supplemented with 10% fetal bovine serum and 10 mM HEPES (PAA Laboratories GmbH).

Imaging

Confocal images were acquired on a Leica SP8 microscope with 40 \times , 1.2 NA water immersion objective corrected for 0.17 mm coverslip thickness. tICS movies with 200 images with a pixel size of 0.18 μm were acquired at the frame rate of 1.17 image per second. Fluorescence excited with the 488-nm laser line was filtered using a tunable 505- to 560-nm bandpass filter and detected with a hybrid detector (HyD) in photon-counting mode.

Immunofluorescence images were obtained by merging at least 20 cells per condition. Images were realigned using the micropattern as a reference, visualize by adding fluorescent fibrinogen-Alexa546 (Sigma). Images acquired using 561- or 633-nm excitation laser beam were filtered using the spectra advised by the manufacturer and detected with the HyD detector.

tICS analysis

tICS movies of 200 images recorded at 0.87 fps were analyzed using a MATLAB program (The MathWorks, Natick, MA), adapted from the principle described by Wiseman *et al.* (2000). Segmentation of images was made by combining two threshold values to determine first the pixels corresponding to the background around the cell, then to select the pixels assigned to the FA. The pixels were eventually sorted to different tensional regions of the cells according to their position in respect to disks and semidisks of 7 μm in diameter, located at each corner of the patterned cells: the red (head) and blue (tail) disks respectively correspond to regions of low and high level of tension. The two disks located at the barbs of the arrow shape have been cut in two semidisks, orange and purple that we assume to respectively correspond to low and high level of tension, because of their position in respect to the stress fibers. It is worth noting that the analysis could not be performed on a pixel per pixel basis, due to insufficient S/N. Rather, the tICS data were averaged over the above-mentioned tensional regions and then fitted with an interaction model, providing three readout parameters: g_0 , g_∞ , and τ_{off} . The latter is the residence time of integrins, while g_0 and g_∞ are related to the total number (N_{tot}) of integrins in the confocal observation volume, the fraction α_{eq} of those proteins that are in dynamic equilibrium between bound and free (diffusing) state and F_b^{eq} , the bound fraction within this pool at equilibrium. Residence times shorter in adhesion site than outside were rejected, together with those longer than 1000 s.

Statistical analysis

Statistical analyses were performed with the software Origin (OriginLab Corp.) using Student's *t* test. The range of *p* values is represented as follows: n.s., $p > 0.05$, * $p < 0.05$, ** $p < 0.005$, *** $p < 0.0005$. Error bars represent the SD.

ACKNOWLEDGMENTS

This work was funded by ANR and by LLNC as "Equipe labellisée Ligue 2014." R.D.M. was funded by GDR 2588 and the Ministère de la Recherche (MENRT fellowship).

REFERENCES

- Albiges-Rizo C, Destaing O, Fourcade B, Planus E, Block MR (2009). Actin machinery and mechanosensitivity in invadopodia, podosomes and focal adhesions. *J Cell Sci* 122, 3037–3049.
- Anthis NJ, Haling JR, Oxley CL, Memo M, Wegener KL, Lim CJ, Ginsberg MH, Campbell ID (2009). Beta integrin tyrosine phosphorylation is a conserved mechanism for regulating talin-induced integrin activation. *J Biol Chem* 284, 36700–36710.
- Arias-Salgado EG, Lizano S, Sarkar S, Brugge JS, Ginsberg MH, Shattil SJ (2003). Src kinase activation by direct interaction with the integrin beta cytoplasmic domain. *Proc Natl Acad Sci USA* 100, 13298–13302.
- Arnold M, Hirschfeld-Warneken VC, Lohmuller T, Heil P, Blummel J, Cavalcanti-Adam EA, Lopez-Garcia M, Walther P, Kessler H, Geiger B, et al. (2008). Induction of cell polarization and migration by a gradient of nanoscale variations in adhesive ligand spacing. *Nano Lett* 8, 2063–2069.
- Bachir AI, Zareno J, Moissoglu K, Plow EF, Gratton E, Horwitz AR (2014). Integrin-associated complexes form hierarchically with variable stoichiometry in nascent adhesions. *Curr Biol* 24, 1845–1853.
- Ballestrem C, Hinz B, Imhof BA, Wehrle-Haller B (2001). Marching at the front and dragging behind: differential alphaVbeta3-integrin turnover regulates focal adhesion behavior. *J Cell Biol* 155, 1319–1332.
- Bledzka K, Bialkowska K, Nie H, Qin J, Byzova T, Wu C, Plow EF, Ma YQ (2010). Tyrosine phosphorylation of integrin beta3 regulates kindlin-2 binding and integrin activation. *J Biol Chem* 285, 30370–30374.
- Bourgeois D, Regis-Faro A, Adam V (2012). Photoactivated structural dynamics of fluorescent proteins. *Biochem Soc Trans* 40, 531–538.
- Brakebusch C, Grose R, Quondamatteo F, Ramirez A, Jorcano JL, Pirro A, Svensson M, Herken R, Sasaki T, Timpl R, et al. (2000). Skin and hair follicle integrity is crucially dependent on beta 1 integrin expression on keratinocytes. *EMBO J* 19, 3990–4003.
- Bureau L, Balland M (2014). Thermosensitive micropatterned substrates. *Methods Cell Biol* 120, 145–154.
- Cairo CW, Mirchev R, Golan DE (2006). Cytoskeletal regulation couples LFA-1 conformational changes to receptor lateral mobility and clustering. *Immunity* 25, 297–308.
- Calderwood DA, Fujioka Y, de Pereda JM, Garcia-Alvarez B, Nakamoto T, Margolis B, McGlade CJ, Liddington RC, Ginsberg MH (2003). Integrin beta cytoplasmic domain interactions with phosphotyrosine-binding domains: a structural prototype for diversity in integrin signaling. *Proc Natl Acad Sci USA* 100, 2272–2277.
- Case LB, Baird MA, Shtengel G, Campbell SL, Hess HF, Davidson MW, Waterman CM (2015). Molecular mechanism of vinculin activation and nanoscale spatial organization in focal adhesions. *Nat Cell Biol* 17, 880–892.
- Case LB, Waterman CM (2015). Integration of actin dynamics and cell adhesion by a three-dimensional, mechanosensitive molecular clutch. *Nat Cell Biol* 17, 955–963.
- Chen L, Vicente-Manzanares M, Potvin-Trottier L, Wiseman PW, Horwitz AR (2012). The integrin-ligand interaction regulates adhesion and migration through a molecular clutch. *PLoS One* 7, e40202.
- Cluzel C, Saltel F, Lussi J, Paulhe F, Imhof BA, Wehrle-Haller B (2005). The mechanisms and dynamics of (alpha)v(beta)3 integrin clustering in living cells. *J Cell Biol* 2, 383–92.
- Czuchra A, Meyer H, Legate KR, Brakebusch C, Fassler R (2006). Genetic analysis of beta1 integrin “activation motifs” in mice. *J Cell Biol* 174, 889–899.
- Datta A, Huber F, Boettiger D (2002). Phosphorylation of beta3 integrin controls ligand binding strength. *J Biol Chem* 277, 3943–3949.
- Deshmukh L, Gorbatyuk V, Vinogradova O (2010). Integrin {beta}3 phosphorylation dictates its complex with the Shc phosphotyrosine-binding (PTB) domain. *J Biol Chem* 285, 34875–34884.
- Destaing O, Block MR, Planus E, Albiges-Rizo C (2011). Invadosome regulation by adhesion signaling. *Curr Opin Cell Biol* 23, 597–606.
- Destaing O, Planus E, Bouvard D, Oddou C, Badowski C, Bossy V, Raducanu A, Fourcade B, Albiges-Rizo C, Block MR (2010). beta1A integrin is a master regulator of invadosome organization and function. *Mol Biol Cell* 21, 4108–4119.
- Elloumi-Hannachi I, Garcia JR, Shekeran A, Garcia AJ (2015). Contributions of the integrin beta1 tail to cell adhesive forces. *Exp Cell Res* 332, 212–222.
- Elosegui-Artola A, Bazellières E, Allen MD, Andreu I, Oria R, Sunyer R, Gomm JJ, Marshall JF, Louise Jones J, Treppe X, Roca-Cusachs P (2014). Rigidity sensing and adaptation through regulation of integrin types. *Nat Mat* 13, 631–637.
- Ferguson SM, Raimondi A, Paradise S, Shen H, Mesaki K, Ferguson A, Destaing O, Ko G, Takasaki J, Cremona O, et al. (2009). Coordinated actions of actin and BAR proteins upstream of dynamin at endocytic clathrin-coated pits. *Dev Cell* 17, 811–822.
- Fourcade B (2017). Fluctuation correlation models for receptor immobilization. *Phys Rev E* 96, 062403.
- Galior K, Liu Y, Yehl K, Vivek S, Salaita K (2016). Titin-based nanoparticle tension sensors map high-magnitude integrin forces within focal adhesions. *Nano Lett* 16, 341–348.
- Giannone G, Sheetz MP (2006). Substrate rigidity and force define form through tyrosine phosphatase and kinase pathways. *Trends Cell Biol* 16, 213–223.
- Ha T, Tinnefeld P (2012). Photophysics of fluorescent probes for single-molecule biophysics and super-resolution imaging. *Annu Rev Phys Chem* 63, 595–617.
- Hoffmann JE, Fermin Y, Stricker RL, Ickstadt K, Zamir E (2014). Symmetric exchange of multi-protein building blocks between stationary focal adhesions and the cytosol. *Elife* 3, e02257.
- Horton ER, Humphries JD, James J, Jones MC, Askari JA, Humphries MJ (2016). The integrin adhesome network at a glance. *J Cell Sci* 129, 4159–4163.
- Huveneers S, Danen EH (2009). Adhesion signaling—crosstalk between integrins, Src and Rho. *J Cell Sci* 122, 1059–1069.
- Kolin DL, Ronis D, Wiseman PW (2006). k-Space image correlation spectroscopy: a method for accurate transport measurements independent of fluorophore photophysics. *Biophys J* 91, 3061–3075.
- Kolin DL, Wiseman PW (2007). Advances in image correlation spectroscopy: measuring number densities, aggregation states, and dynamics of fluorescently labeled macromolecules in cells. *Cell Biochem Biophys* 49, 141–164.
- Law DA, DeGuzman FR, Heiser P, Ministri-Madrid K, Killeen N, Phillips DR (1999). Integrin cytoplasmic tyrosine motif is required for outside-in alphaIIb beta3 signalling and platelet function. *Nature* 401, 808–811.
- Law DA, Nannizzi-Alaimo L, Phillips DR (1996). Outside-in integrin signal transduction. Alpha IIb beta 3-(GP IIb IIIa) tyrosine phosphorylation induced by platelet aggregation. *J Biol Chem* 271, 10811–10815.
- Leduc C, Si S, Gautier J, Soto-Ribeiro M, Wehrle-Haller B, Gautreau A, Giannone G, Cognet L, Lounis B (2013). A highly specific gold nanoprobe for live-cell single-molecule imaging. *Nano Lett* 13, 1489–1494.
- Liao Z, Kato H, Pandey M, Cantor JM, Ablooglu AJ, Ginsberg MH, Shattil SJ (2015). Interaction of kindlin-2 with integrin beta3 promotes outside-in signaling responses by the alphaVbeta3 vitronectin receptor. *Blood* 125, 1995–2004.
- Lin GL, Cohen DM, Desai RA, Breckenridge MT, Gao L, Humphries MJ, Chen CS (2013). Activation of beta 1 but not beta 3 integrin increases cell traction forces. *FEBS Lett* 587, 763–769.
- Mandal K, Wang I, Vitiello E, Orellana LA, Balland M (2014). Cell dipole behaviour revealed by ECM sub-cellular geometry. *Nat Commun* 5, 5749.
- Martel V, Racaud-Sultan C, Dupe S, Marie C, Paulhe F, Galmiche A, Block MR, Albiges-Rizo C (2001). Conformation, localization, and integrin binding of talin depend on its interaction with phosphoinositides. *J Biol Chem* 276, 21217–21227.
- Milloud R, Destaing O, de Mets R, Bourrin-Reynard I, Oddou C, Delon A, Wang I, Albiges-Rizo C, Balland M (2017). alphaVbeta3 integrins negatively regulate cellular forces by phosphorylation of its distal NPXY site. *Biol Cell* 109, 127–137.
- Moore SW, Roca-Cusachs P, Sheetz MP (2010). Stretchy proteins on stretchy substrates: the important elements of integrin-mediated rigidity sensing. *Dev Cell* 19, 194–206.
- Oxley CL, Anthis NJ, Lowe ED, Vakonakis I, Campbell ID, Wegener KL (2008). An integrin phosphorylation switch: the effect of beta3 integrin tail phosphorylation on Dok1 and talin binding. *J Biol Chem* 283, 5420–5426.
- Pines M, Das R, Ellis SJ, Morin A, Czerniecki S, Yuan L, Klose M, Coombs D, Tanentzapf G (2012). Mechanical force regulates integrin turnover in *Drosophila* in vivo. *Nat Cell Biol* 14, 935–943.
- Plotnikov SV, Pasapera AM, Sabass B, Waterman CM (2012). Force fluctuations within focal adhesions mediate ECM-rigidity sensing to guide directed cell migration. *Cell* 151, 1513–1527.
- Rahmouni S, Lindner A, Rechenmacher F, Neubauer S, Sobahi TR, Kessler H, Cavalcanti-Adam EA, Spatz JP (2013). Hydrogel micropillars with integrin selective peptidomimetic functionalized nanopatterned tops: a new tool for the measurement of cell traction forces transmitted through alphavbeta3- or alpha5beta1-integrins. *Adv Mater* 25, 5869–5874.

- Roca-Cusachs P, Gauthier NC, Del Rio A, Sheetz MP (2009). Clustering of alpha(5)beta(1) integrins determines adhesion strength whereas alpha(v)beta(3) and talin enable mechanotransduction. *Proc Natl Acad Sci USA* 106, 16245–16250.
- Rossier O, Ochteau V, Sibarita JB, Leduc C, Tessier B, Nair D, Gatterdam V, Destaing O, Albiges-Rizo C, Tampe R, et al. (2012). Integrins beta1 and beta3 exhibit distinct dynamic nanoscale organizations inside focal adhesions. *Nat Cell Biol* 14, 1057–1067.
- Schaffner-Reckinger E, Brons NH, Kieffer N (2001). Evidence from site-directed mutagenesis that the cytoplasmic domain of the beta3 subunit influences the conformational state of the alphaVbeta3 integrin ectodomain. *Thromb Haemost* 85, 716–723.
- Schaffner-Reckinger E, Gouon V, Melchior C, Plancon S, Kieffer N (1998). Distinct involvement of beta3 integrin cytoplasmic domain tyrosine residues 747 and 759 in integrin-mediated cytoskeletal assembly and phosphotyrosine signaling. *J Biol Chem* 273, 12623–12632.
- Schaller MD, Otey CA, Hildebrand JD, Parsons JT (1995). Focal adhesion kinase and paxillin bind to peptides mimicking beta integrin cytoplasmic domains. *J Cell Biol* 130, 1181–1187.
- Schiller HB, Hermann MR, Polleux J, Vignaud T, Zanivan S, Friedel CC, Sun Z, Raducanu A, Gottschalk KE, Thery M, et al. (2013). beta1- and alphaV-class integrins cooperate to regulate myosin II during rigidity sensing of fibronectin-based microenvironments. *Nat Cell Biol* 15, 625–636.
- Schwartzberg PL, Xing L, Hoffmann O, Lowell CA, Garrett L, Boyce BF, Varmus HE (1997). Rescue of osteoclast function by transgenic expression of kinase-deficient Src in src^{-/-} mutant mice. *Genes Dev* 11, 2835–2844.
- Thery M, Pepin A, Dressaire E, Chen Y, Bornens M (2006). Cell distribution of stress fibres in response to the geometry of the adhesive environment. *Cell Motil Cytoskeleton* 63, 341–355.
- Toplak T, Pandzic E, Chen L, Vicente-Manzanares M, Horwitz AR, Wiseman PW (2012). STICCS reveals matrix-dependent adhesion slipping and gripping in migrating cells. *Biophys J* 103, 1672–1682.
- Trappmann B, Gautrot JE, Connelly JT, Strange DG, Li Y, Oyen ML, Cohen Stuart MA, Boehm H, Li B, Vogel V, et al. (2012). Extracellular-matrix tethering regulates stem-cell fate. *Nat Mater* 11, 642–649.
- Tseng Q, Wang I, Duchemin-Pelletier E, Azioune A, Carpi N, Gao J, Filhol O, Piel M, Thery M, Balland M (2011). A new micropatterning method of soft substrates reveals that different tumorigenic signals can promote or reduce cell contraction levels. *Lab Chip* 11, 2231–2240.
- Wehrle-Haller B (2007). Analysis of integrin dynamics by fluorescence recovery after photobleaching. *Methods Mol Biol* 370, 173–202.
- Winograd-Katz SE, Fässler R, Geiger B, Legate KR (2014). The integrin adhesome: from genes and proteins to human disease. *Nat Rev Mol Cell Biol* 15, 273–288.
- Wiseman PW, Squier JA, Ellisman MH, Wilson KR (2000). Two-photon image correlation spectroscopy and image cross-correlation spectroscopy. *J Microsc* 200 (Pt 1), 14–25.
- Worth DC, Hovalala-Dilke K, Robinson SD, King SJ, Morton PE, Gertler FB, Humphries MJ, Parsons M (2010). Alpha v beta3 integrin spatially regulates VASP and RIAM to control adhesion dynamics and migration. *J Cell Biol* 189, 369–383.
- Yu CH, Rafiq NB, Cao F, Zhou Y, Krishnasamy A, Biswas KH, Ravasio A, Chen Z, Wang YH, Kawauchi K, et al. (2015). Integrin-beta3 clusters recruit clathrin-mediated endocytic machinery in the absence of traction force. *Nat Commun* 6, 8672.